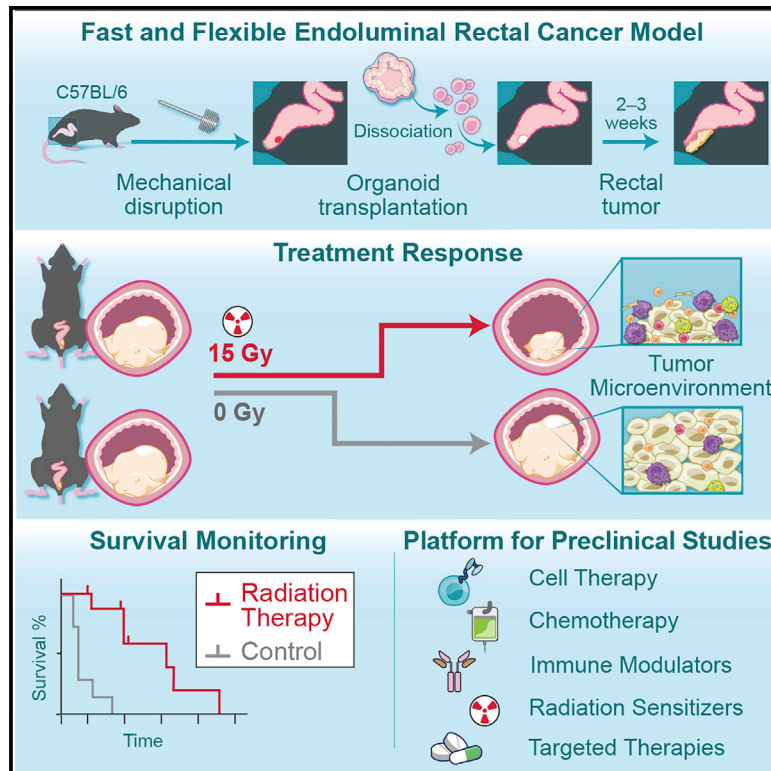Report

An immunocompetent rectal cancer model to study radiation therapy

Graphical abstract

Authors

Jin K. Kim, Chao Wu, Michael Del Latto, ..., Julio García-Aguilar, Paul B. Romesser, J. Joshua Smith

Correspondence

romessep@mskcc.org (P.B.R.), smithj5@mskcc.org (J.J.S.)

In brief

Kim et al. demonstrate an immunocompetent rectal cancer implantation model that avoids the use of dextran sulfate sodium. Using this approach, orthotopically transplanted tumors can be used for rapid preclinical screening of radiosensitizers, immunomodulators, and other therapies emerging in cancer treatment and research.

Highlights

- An immunocompetent endoluminal rectal cancer murine model

- Engraftment is based on mechanical disruption

- Tumors recapitulate anatomical origin, histology, and response to radiation

- Ease of use and physiological relevance can improve preclinical therapy modeling

CellPress

Report

An immunocompetent rectal cancer model to study radiation therapy

Jin K. Kim,[1,11] Chao Wu,[1,2,11] Michael Del Latto,[3,11] Yajing Gao,[1,2,10,11] Seo-Hyun Choi,[1] Maria Kierstead,[3] Charles-Etienne Gabriel Sauvé,[1] Canan Firat,[4] Almudena Chaves Perez,[5] Jussi Sillanpaa,[6] Chin-Tung Chen,[1] Kayla E. Lawrence,[2] Philip B. Paty,[1] Francisco M. Barriga,[5] John E. Wilkinson,[7] Jinru Shia,[4] Charles L. Sawyers,[2,8] Scott W. Lowe,[5,8] Julio García-Aguilar,[1] Paul B. Romesser,[3,9,12,*] and J. Joshua Smith[1,2,13,14,*]

[1]Colorectal Service, Department of Surgery, Memorial Sloan Kettering Cancer Center, New York, NY 10065, USA
[2]Human Oncology and Pathogenesis Program, Memorial Sloan Kettering Cancer Center, New York, NY 10065, USA
[3]Department of Radiation Oncology, Memorial Sloan Kettering Cancer Center, New York, NY 10065, USA
[4]Department of Pathology, Memorial Sloan Kettering Cancer Center, New York, NY 10065, USA
[5]Cancer Biology and Genetics Program, Sloan Kettering Institute, Memorial Sloan Kettering Cancer Center, New York, NY 10065, USA
[6]Department of Medical Physics, Memorial Sloan Kettering Cancer Center, New York, NY 10065, USA
[7]Department of Pathology, University of Michigan, Ann Arbor, MI 48109, USA
[8]Howard Hughes Medical Institute, Memorial Sloan Kettering Cancer Center, New York, NY 10065, USA
[9]Early Drug Development Service, Department of Medicine, Memorial Sloan Kettering Cancer Center, New York, NY 10065, USA
[10]Present address: College of Food Science and Technology, Huazhong Agricultural University, Wuhan 430070, China
[11]These authors contributed equally
[12]Twitter: @DrPaulRomesser
[13]Twitter: @JoshSmithMDPhD
[14]Lead contact
*Correspondence: romessep@mskcc.org (P.B.R.), smithj5@mskcc.org (J.J.S.)
https://doi.org/10.1016/j.crmeth.2022.100353

MOTIVATION Rectal cancer (RC) incidence is increasing worldwide, especially among young adults 50 years of age and younger.[40–46] The complexity of treatment highlights the need for the development of rapid models that can be used to better understand the biology of RC and to conduct robust preclinical studies. Current, approaches utilize induction by dextran sulfate sodium (DSS), which alters the immune physiology of the microenvironment, or models in which tumor origin occurs from the submucosa, which is not the typical site of disease origin. These limitations are particularly important as recent reports suggest that the underlying biology and genetics of inflammatory-associated colorectal tumors are distinct from non-inflammatory tumors.[47] How or to what extent DSS treatment influences this is unknown, but the systemic side effects are a concern, and development of a simpler and faster, DSS-free model would be helpful to disentangle these factors. We therefore sought to develop a more anatomically and physiologically relevant RC murine model that is straightforward and rapid. The model described here relies on simple mechanical disruption of the target tissue, rather than DSS treatment, and localizes engraftment to the mucosal tissue, which better reflects the anatomical origin of this tumor type.

SUMMARY

We describe a mouse model of rectal cancer (RC) involving rapid tumor organoid engraftment via orthotopic transplantation in an immunocompetent setting. This approach uses simple mechanical disruption to allow engraftment, avoiding the use of dextran sulfate sodium. The resulting RC tumors invaded from the mucosal surface and metastasized to distant organs. Histologically, the tumors closely resemble human RC and mirror remodeling of the tumor microenvironment in response to radiation. This murine RC model thus recapitulates key aspects of human RC pathogenesis and presents an accessible approach for more physiologically accurate, preclinical efficacy studies.

INTRODUCTION

Rectal cancer (RC) constitutes approximately one-third of colorectal cancer diagnoses and increasingly affects younger individuals (<50 years old).[1] Rectal cancer is typically treated with radiotherapy (RT) and, if necessary, chemotherapy before radical surgery. Historically, RT sensitivity has largely been considered a cell-intrinsic property resulting from indirect and direct DNA damage, yet tumor genetics alone do not fully explain RT sensitivity. There is growing evidence that immune effects significantly contribute to RT sensitivity. The immune tumor microenvironment (TME) plays a crucial role in tumorigenesis and response to treatment.[2–5] In turn, RT, by inducing DNA damage and cell death, may induce TME remodeling[5] and modulate immunological responses.[4,6,7] Investigating these ideas will require immunocompetent murine models that accurately mimic human RC and its response to RT. These models should also provide an opportunity to develop novel effective therapy regimens involving immunomodulators for the treatment of RC, which has been reported relatively less sensitive to the current immunotherapy compared with right-sided colorectal cancer.[8]

Numerous murine models of colon cancer have been established, but these do not offer an ideal setting in which to examine the TME for RC as the pelvic anatomy and blood supply are unique. A limited number of murine models have been developed in the proper rectal anatomic context, but these involve either chemical induction—a method that Yui et al. utilized successfully to implant colonic organoids orthotopically[9]—which can cause chronic colitis and alter the TME, or intrarectal injection of tumor cells, which results in submucosal-initiated tumors, unlike human tumors that initiate in the mucosa.[10,11] The advantages and limitations of existing models are summarized in Table 1.

There is an additional need for optimized RT delivery methods within murine RC models. Many studies have used whole-body radiation, which is a common treatment for patients, but this is not representative of localized pelvic RT and adds undesirable systemic effects.[30,31] Recent studies such as that performed by Nicolas et al. have shown that fractionated radiotherapy in combination with immunotherapy/Il-1α can be used in orthotopic immunocompetent RC models to administer RT treatment with clinical precision,[32,33] but this is limited by complexity of which medical devices and technology are required. As such, we sought to develop an anatomically and physiologically accurate RC model, along with a widely adaptable pelvic irradiation method that better meets the needs presented above.

RESULTS AND DISCUSSION

We isolated and cultured organoids from genetically engineered ($Apc^{flox/flox}$, LSL-$Kras^{G12D/+}$, $Tp53^{flox/flox}$) mouse (C57Bl/6J) rectal tissue. Organoids were transduced ex $vivo$ with adeno viral vector expressing Cre-recombinase to activate Kras and inactivate Apc and p53 ($Apc^{-/-}$, $Kras^{G12D/+}$, $Tp53^{-/-}$; hereafter referred to as AKP).[20,22] This represents a common genetic configuration in human RC.[34] Organoids of the desired genotype were selected by removing WNT ligands and epidermal growth factor from the media, followed by Nutlin-3 selection.[10]

The resulting AKP rectal tumor organoids (tumoroids) were prepared as an enema. Mice (C57Bl/6J) were anesthetized, and a small-caliber brush was inserted through the anus to mechanically disrupt the rectal mucosa (Figures 1A and 1B). Thereafter, tumoroids were transanally instilled into the rectum, and the anus was glued shut for 6–8 h to prevent expulsion and facilitate tumoroid engraftment. Step-by-step instructions are provided in Video S1. Of note, the technical aspects of our tumor engraftment procedure are simpler compared with surgical or endoscopic implantation protocols and thus easily adoptable by other investigators. Compared with DSS models that can result in multifocal or segmental lesions[35] and potentially implant tumors anywhere along the colonic tract, our method has less of a systemic inflammatory response and reliably engrafts tumors in the rectum. It is important to note that mechanical disruption reduces anesthesia time compared with methods involving surgical procedures. Animal stress is also reduced compared with DSS methods as the animal does not exhibit a systemic inflammatory state, recovers quickly, and does not require significant delays prior to potential experimental alterations such as treatment with radiation once the tumors engraft. This method allows animals to be engrafted in a manner that is fast, efficient, and well tolerated, enabling larger scale experiments to be performed. Tumoroids engraft at the site of mucosal disruption (Figure 1C) and preserve WNT and KRAS pathways alterations in $vivo$, as demonstrated by elevated β-catenin and phospho-ERK (Figures S1A and S1B).

Of 118 mice treated, 20 (17%) died within 2 days after transplantation due to intestinal perforation (confirmed at autopsy). Among the 98 surviving mice, this procedure yielded a 58% engraftment rate (Figure 1A, right panel). We have compared the engraftment rate of different RC models carefully in Table 1. The engraftment rate of this model is close to the immunocompetent model discussed (62%).[10] Higher engraftment rates are seen across immunocompromised models.[25,27,29] Tumor engraftment (seen by either a luminal mass or increasing size of a luminal lesion) was apparent on colonoscopy by 2–4 weeks after transplantation (Figure 1D). The median distance of the tumor from the anal verge was 3.5 mm (range, 0–10 mm) (Figure 1E). Engrafted tumors grew and obstructed the rectal lumen within 1–3 months of transplantation (Figure 1D) and were macroscopically similar to human RC under endoscopy (Figure 1F). In rare cases histopathologic review showed that the engrafted tumors resemble the development and progression from pre-invasive to invasive cancer and to metastatic disease (Figures 1H and 1I) as observed in human RC (Figure 1G). These data establish the feasibility of this RC model and its clinically relevant patterns of tumor progression and metastasis.

To test the application of RT to our model, we administered localized pelvic RT (Figures 2A and 2B) to tumor-bearing mice using a customized Cerrobend holding apparatus (Figures S2A–S2D). Mice were randomized at a median of 5 weeks after transplantation with no difference in average tumor size between cohorts (Figures S1C and S1D). Mice in the RT cohort underwent localized pelvic radiation to 15 Gy in a single fraction. All mice were monitored carefully for health status and subjected to weekly surveillance endoscopy. Euthanasia occurred when the circumferential tumor involvement exceeded 50% of the rectal lumen.

Table 1. Colon and rectal cancer mouse models by anatomic relevance

Anatomic location	Tumorigenesis method	Advantages	Disadvantages	Engraftment rate	Reference
Heterotopic methods					
Subcutaneous flank	tumor injection	• technically simple	• ectopic micro-environment • does not metastasize	25%, 81%[12] 56%[13]	Drost et al.[12]; Rivera et al.[13]
Abdominal organ (Renal capsule, peritoneum)	tumor injection	• high engraftment	• ectopic micro-environment • immunocompromised host		Tanaka et al.[14]; Schoffelen et al.[15]
Orthotopic methods—colon					
Cecum	surgical submucosal implantation of tumor	• high engraftment • immunocompetent host	• requires surgical technical expertise • intestinal tumoroids inserted from the serosal side of the bowel	100%[16]	Fumagalli et al.[16]
Predominantly colon	colitis-induced	• inexpensive • can be used in mice with any genetic background	• mimics colitis-associated colorectal cancer, not sporadic colorectal cancer • tumor location is not specific to rectum • slow tumor growth (10–30 weeks until tumor formation)	38%–100%[17] 80%–100%[18]	Tanaka et al.[17]; Neufert et al.[18]
Predominantly colon	genetically modified murine model	• mimics sporadic cancer • immunocompetent host	• tumorigenesis in multiple organs; location not specific to rectum • expensive as it requires genetically engineered mice	20%–50%[19]	Dow et al.[19]; Xue et al.[19,20]
Distal colon	genetically modified murine model with focal activation of mutations	• mimics sporadic cancer • metastasis reported	• expensive as it requires genetically engineered mice • slow tumor growth (≥10 weeks until >20% lumen obstruction)	71%–96%[21] 34%–92%[22]	Roper et al.[21]; Hung et al.[22]

(Continued on next page)

Table 1. *Continued*

Anatomic location	Tumorigenesis method	Advantages	Disadvantages	Engraftment rate	Reference
Distal colon	colonoscopy-based mural injection of tumor	• high engraftment • metastasis reported	• technically challenging • tumor does not initiate from the mucosa	83%[23] 90%–92%[24]	Bettenworth et al.[23]; Roper et al.[24]
Orthotopic methods—rectum					
Distal colon and rectum	colitis induction + tumor enema	• tumors grow from the mucosal lumen • metastasis reported • applicable to immunocompetent host	• chemically induced colitis alters the tumor microenvironment • multifocal tumor formation along the colorectum • tumorigenesis: weeks to months	100%[25] 20%–100%[26] 94%[27] 62%[10]	O'Rourke et al.[10]; Kishimoto et al.[25]; Takahashi et al.[26]; Ganesh et al.[27]; Chassaing et al.[28]
Rectum	intrarectal tumor injection	• tumors form in distal rectum (1–2 mm above anus) • high engraftment • applicable to immunocompetent host	• tumor does not initiate from the mucosa • tumors are too close to the anus for endoluminal monitoring, so they need to be tagged with bioluminescent markers for imaging	100%[29]	Kasashima et al.[11]; Hite et al.[29]

Prolapse, a common negative outcome for other similar models,[36] was not observed in any of our implanted mice (n = 118). Mice tolerated RT well without significant weight loss or illness. We also compared the survival rate between pelvic-irradiated mice and whole-body irradiated mice to ensure our localized pelvic RT system provided effective bone marrow shielding and mitigated lethality from whole-body irradiation (Figure S2E).

A 10%–40% treatment effect was seen after RT on histological examination and tumor regression grading. This treatment effect is similar to what we see in RC patients.[37,38] A significant growth delay was noted, endoscopically, after RT, but most mice eventually experienced tumor growth (Figures 2C and 2D). Mice treated with localized pelvic RT had significantly improved survival (Figure 2E).

We sought to evaluate if our model recapitulates changes in the TME in response to RT as it does in human patients. Prior research has shown a significant increase in M2 macrophage polarization in human rectal tumors postRT.[39] Similarly, when examining the TME of mice with *AKP* endoluminal tumors, we observed a significant increase in macrophage infiltration (detected by macrophage surface marker F4/80) and M2 polariza-

tion (CD206⁺ F4/80⁺), but not M1 (CD11c⁺ F4/80⁺) (Figures 2F–2H). These data suggest that our model reflects some key changes in the TME and its response to RT.

In summary, this model has a wide range of potential preclinical applications, such as the evaluation of radiosensitizers, combinations of RT with immunomodulators, and novel therapies. Furthermore, this model can be used to explore how RT resistance is affected by various oncogenic mutations. For any of these applications, our method provides rapid generation of localized, mucosa-initiated rectal tumors in a model that is reliable, reproducible, and translatable to human RC with limited technical demand.

Limitations of study

Injury to the rectal mucosa without internal visual guidance may result in occasional unintended perforation of the bowel wall. Perforation may occur from a myriad of different factors, but from a technical standpoint, it can be commonly attributed to the following: over-brushing the epithelium, applying excess pressure when causing abrasion, inserting the brush too deep or too quickly into the rectum, insufficient
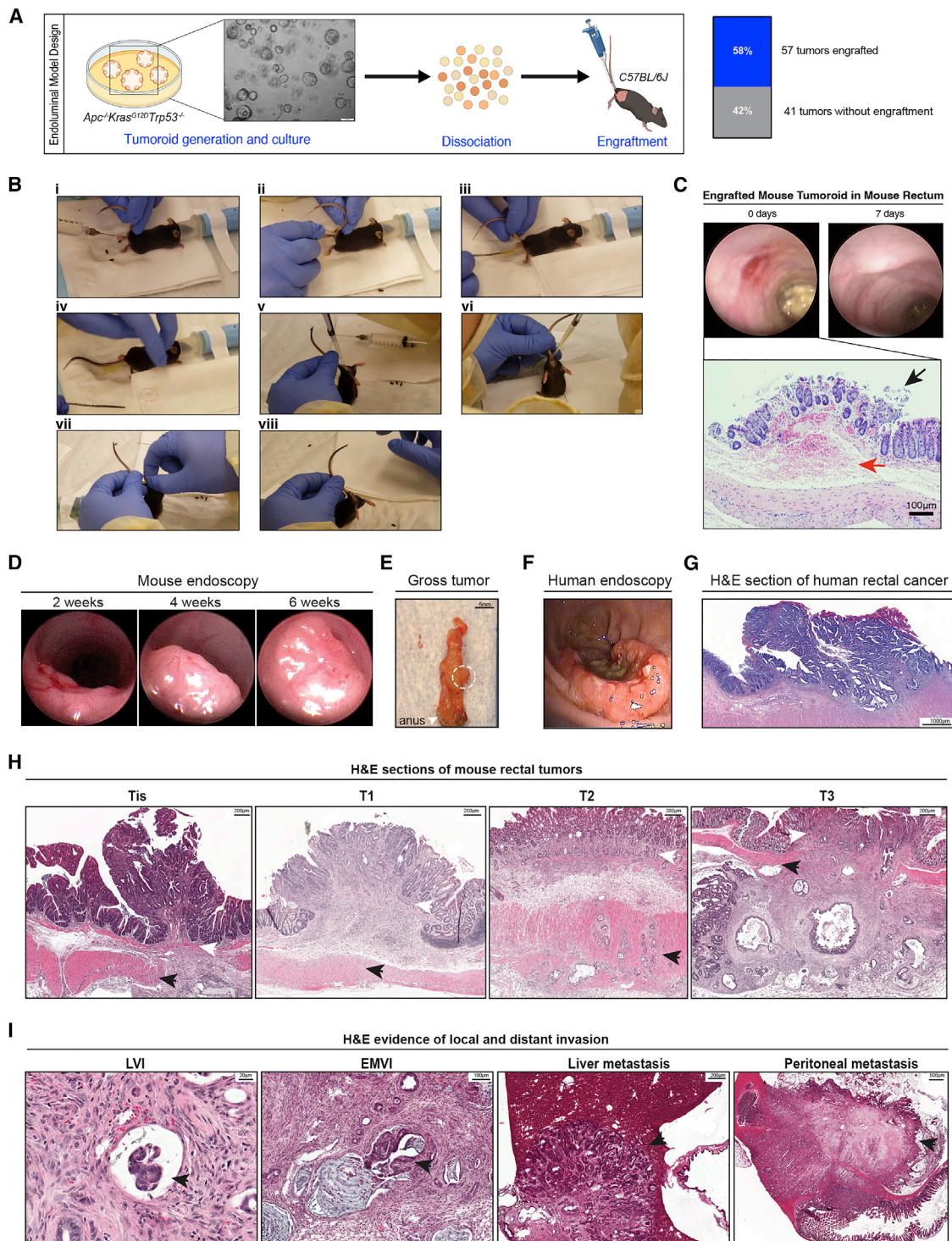
Figure 1. An orthotopic rectal cancer model in immunocompetent mice

(A) Diagram of rectal tumoroid preparation for orthotopic transplantation. *AKP* rectal organoids were cultured in Matrigel, harvested, and engrafted as an enema to C57Bl/6J mice after mechanical disruption of the rectal mucosa.

(B) Critical steps in endoluminal engraftment. (1) Irrigate rectum with PBS. (2) Insert a trimmed P200 pipette tip into the anus as a guide. (3) Insert and irritate mucosa with a small-caliber brush. (4) Confirm a blood smear on the brush, which indicates adequate endoluminal disruption. (5) Pipette tumoroid mixture into the rectum. (6) Seal the anus with Vetbond tissue adhesive. (7) Pinch the anus closed. (8) Allow Vetbond to dry and confirm the anus is sealed. See also Video S1.

(legend continued on next page)

lubrication, improper removal of the brush from the rectum, over-application of tissue adhesive, and/or failure to completely remove tissue adhesive. The procedural mortality rate in our study was 17%. These percentages are reasonable estimates for inexperienced users and should be considered when proposing animal numbers for use and justification. It is important to account for procedural mortality when planning experiments as it impacts mice available for engraftment. Through the course of ongoing experiments beyond the scope of the current paper, we have found that training and experience substantially decreases procedural mortality. As with any new technique, we encourage discussion with the animal use and welfare committee. It is critical to have an approved protocol prior to application of this technique.

STAR★METHODS

Detailed methods are provided in the online version of this paper and include the following:

- KEY RESOURCES TABLE
- RESOURCE AVAILABILITY
  - Lead contact
  - Materials availability
  - Data and code availability
- EXPERIMENTAL MODEL AND SUBJECT DETAILS
  - Mice
- METHOD DETAILS
  - Culturing and preparation of tumoroids for endoluminal transplantation
  - Mechanical disruption of the mouse rectal mucosa and tumoroid transplantation
  - Tumor surveillance and measuring tumor growth
  - Localized pelvic radiation
  - Histopathology
  - Immunofluorescence
  - Imaging
  - Monitoring mouse health
  - Adherence to established endpoints
- QUANTIFICATION AND STATISTICAL ANALYSIS

SUPPLEMENTAL INFORMATION

Supplemental information can be found online at https://doi.org/10.1016/j.crmeth.2022.100353.

AUTHOR CONTRIBUTIONS

Conceptualization, J.K.K., J.G.A., P.B.R., and J.J.S.; methodology, J.K.K., C.W., M.D., A.C.P., J.S., P.B.R., and J.J.S.; validation, J.K.K., C.W., M.D., Y.G., S.C., and C.C.; formal analysis, J.K.K., Y.G., C.G.S., C.F., J.S., P.B.P., J.E.W., J.S., P.B.R., and J.J.S.; investigation, J.K.K, C.W., and M.D.; resources, J.K.K., C.W., M.D., S.C., C.C., F.M.B., P.B.R., and J.J.S.; data curation, J.K.K., C.W., M.D., and Y.G.; writing – original draft, J.K.K, C.W., M.D., P.B.R., and J.J.S.; writing – review and editing, J.K.K., C.W., M.D., Y.G., S.C., M.K., P.B.R., and J.J.S.; visualization, J.K.K., C.W., M.D., J.G., S.C., C.G.S., C.F., A.C.P., J.S., C.C., K.E.L., P.B.P., J.E.W., J.S., P.B.R., and J.J.S.; supervision, P.B.R. and J.J.S.; project administration, P.B.R. and J.J.S.; funding acquisition, C.L.S., S.W.L., J.G.A., P.B.R., and J.J.S.

DECLARATION OF INTERESTS

C.L.S. serves on the Board of Directors of Novartis, is a co-founder of ORIC Pharmaceuticals and co-inventor of enzalutamide and apalutamide. He is a science advisor to Agios, Arsenal, Beigene, Blueprint, Column Group, Foghorn, Housey Pharma, Nextech, KSQ, and PMV. S.W.L. receives research funding from Calico and is on the scientific advisory boards and holds equity in Blueprint Medicines, Mirimus Inc., ORIC Pharmaceuticals, Geras Bio, Faeth Therapeutics, Senescea Therapeutics, and PMV Pharmaceuticals. He also recently served as a consultant for Boehringer Ingelheim. J.G.A. reports stock ownership in Intuitive Surgical and has served in a consulting or advisory role for Medtronic, Intuitive Surgical, and Johnson & Johnson. P.B.R. reports prior research funding and is a consultant for EMD Serono, receives research funding from XRAD therapeutics, is a consultant for Faeth Therapeutics, is a consultant for Natera, is on the Medical Advisory Board of the HPV Alliance, and is on the Scientific Advisory Board of the Anal Cancer Foundation. J.J.S. received travel support from Intuitive Surgical Inc. (2015) and served as a clinical advisor for Guardant Health Inc. (2019) and Foundation Medicine Inc. (2022). He also served as a consultant and speaker for Johnson & Johnson Inc. (2022).

(C) Tumoroids implanted at the site of mucosal disruption. Endoscopy immediately after brush disruption and 1 week after engrafting shows tumoroids implanting directly at the site of mucosal disruption. H&E stain displays mucosal bleeding, highlighted by the red arrow. The black arrow points to the section of mucosal disruption.

(D) Serial endoscopy pictures of the engrafted tumoroids post-transplantation.

(E) Necropsy shows tumor (circled) in the distal rectum. This tumor was harvested 4 weeks post-transplantation.

(F) A representative endoscopic image of a human rectal cancer. The picture was taken during a flexible sigmoidoscopy.

(G) H&E section of human rectal cancer (from the same tumor with Figure 1F). The T stage for this tumor is pT3.

(H) H&E sections of engrafted tumors in this murine model. Tumors ranging from carcinoma *in situ* (Tis) to T3 are presented. White arrows point to the muscularis mucosa and black arrows to muscularis propria. Representative images are shown; the number of tumors detected for each T stage: n = 3 for Tis, n = 6 for T1, n = 7 for T2, n = 9 for T3.

(I) H&E sections showing local invasion (lymphovascular invasion [LVI] and extramural vascular invasion [EMVI]) and distant metastasis to liver and peritoneum of engrafted tumors. Black arrows point to the tumor. Representative images are shown, n = 2 tumors detected for LVI, n = 1 tumor detected for EMVI, n = 1 tumor detected for both LVI and EMVI.
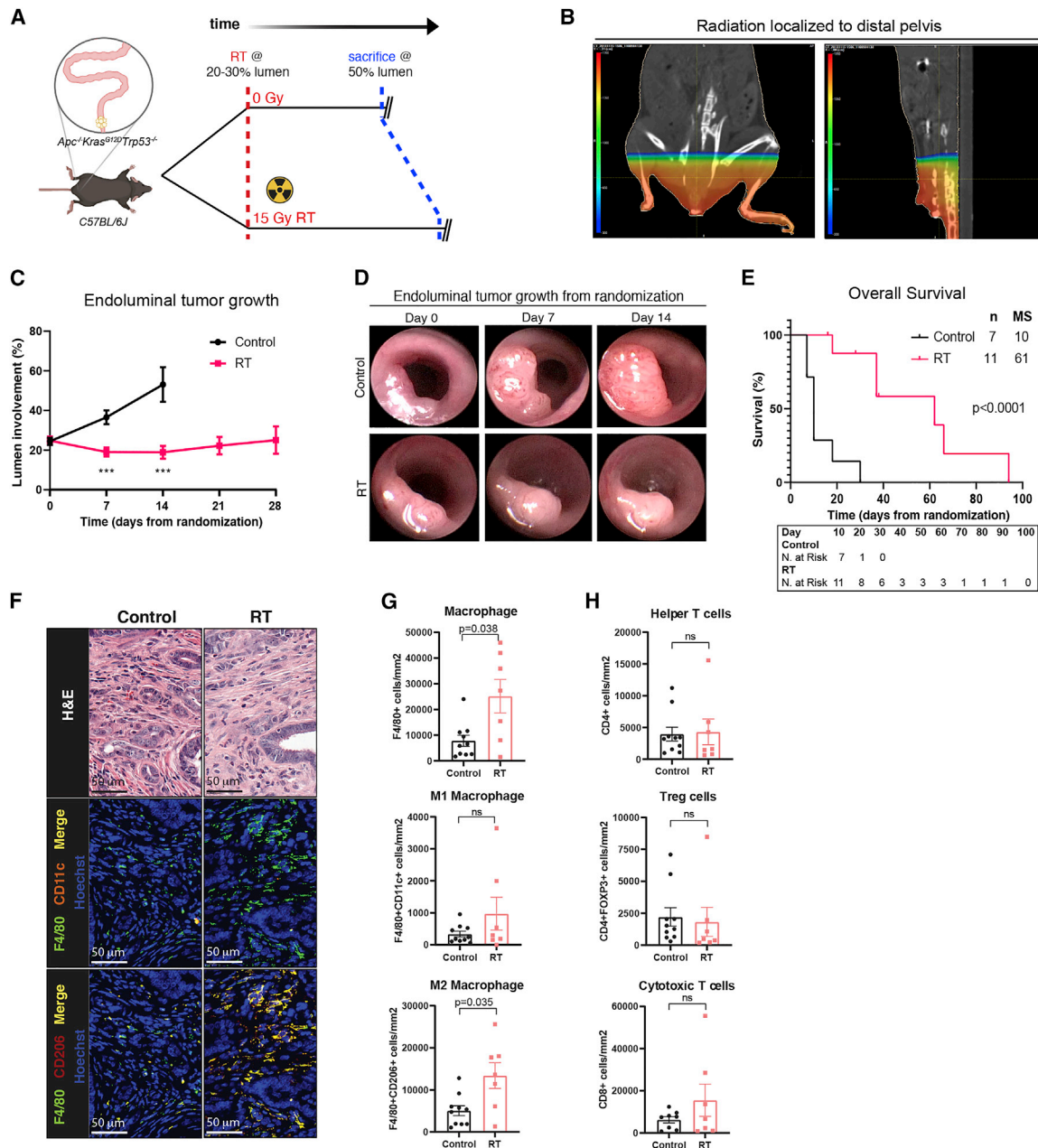
Figure 2. Application and evaluation of localized radiation therapy in the orthotopic rectal cancer mouse model

(A) Experimental schema. See also Figure S2.

(B) Radiation dosimetry of the predicted radiation field to the distal pelvis.

(C) Endoluminal tumor growth. Mean circumferential tumor size of the control and RT group mice at the time of treatment and at weeks 1–4 from treatment are plotted. Error bars denote the standard error of mean. ***$p < 0.0001$ at individual time points by unpaired two-tailed t test.

(D) Representative serial endoscopic pictures of a control mouse and irradiated mouse.

(E) Overall survival of control and RT cohorts. Mice that were sacrificed for having tumor involvement >50% of the lumen were deemed as events. Kaplan-Meier estimates with number at risk depicted; p value for log rank comparison.

(F) Top: representative hematoxylin & eosin (H&E) stained images of rectal tumors from control mouse and irradiated mice. Middle and bottom panels: representative images of immunofluorescent staining for tumor-associated macrophages. F4/80 (green) is a macrophage marker, CD11c (orange) is a marker for M1 polarized macrophages, and CD206 (red) is for M2 polarized; counterstain with Hoechst (blue).

(G) Quantification of tumor-associated macrophages and the M1/M2 subtypes. Each point represents an individual mouse sample. Error bars denote the standard error of mean. p values provided by unpaired two-tailed t test. NS denotes a result that is not statistically significant.

(H) Quantification of $CD4^+$ helper T cells, $CD4^+FOXP3^+$ Treg cells, and $CD8^+$ cytotoxic T cells. Data points, error bars, and p values are as represented as in (G).

REFERENCES

1. Siegel, R.L., Miller, K.D., Fuchs, H.E., and Jemal, A. (2021). Cancer statistics, 2021. CA. Cancer J. Clin. *71*, 7–33. https://doi.org/10.3322/CAAC.21654.

2. Pagès, F., Kirilovsky, A., Mlecnik, B., Asslaber, M., Tosolini, M., Bindea, G., Lagorce, C., Wind, P., Marliot, F., Bruneval, P., et al. (2009). In situ cytotoxic and memory T cells predict outcome in patients with early-stage colorectal cancer. J. Clin. Oncol. *27*, 5944–5951. https://doi.org/10.1200/JCO.2008.19.6147.

3. Anitei, M.G., Zeitoun, G., Mlecnik, B., Marliot, F., Haicheur, N., Todosi, A.M., Kirilovsky, A., Lagorce, C., Bindea, G., Ferariu, D., et al. (2014). Prognostic and predictive values of the immunoscore in patients with rectal cancer. Clin. Cancer Res. *20*, 1891–1899. https://doi.org/10.1158/1078-0432.CCR-13-2830.

4. Kamran, S.C., Lennerz, J.K., Margolis, C.A., Liu, D., Reardon, B., Wankowicz, S.A., Van Seventer, E.E., Tracy, A., Wo, J.Y., Carter, S.L., et al. (2019). Integrative molecular characterization of resistance to neoadjuvant chemoradiation in rectal cancer. Clin. Cancer Res. *25*, 5561–5571. https://doi.org/10.1158/1078-0432.CCR-19-0908.

5. Sia, J., Szmyd, R., Hau, E., and Gee, H.E. (2020). Molecular mechanisms of radiation-induced cancer cell death: a primer. Front. Cell Dev. Biol. *8*, 41. https://doi.org/10.3389/FCELL.2020.00041.

6. Klug, F., Prakash, H., Huber, P.E., Seibel, T., Bender, N., Halama, N., Pfirschke, C., Voss, R.H., Timke, C., Umansky, L., et al. (2013). Low-dose irradiation programs macrophage differentiation to an iNOS$^+$/M1 phenotype that orchestrates effective T cell immunotherapy. Cancer Cell *24*, 589–602. https://doi.org/10.1016/J.CCR.2013.09.014.

7. Apetoh, L., Ghiringhelli, F., Tesniere, A., Obeid, M., Ortiz, C., Criollo, A., Mignot, G., Maiuri, M.C., Ullrich, E., Saulnier, P., et al. (2007). Toll-like receptor 4-dependent contribution of the immune system to anticancer chemotherapy and radiotherapy. Nat. Med. *13*, 1050–1059. https://doi.org/10.1038/NM1622.

8. Baran, B., Mert Ozupek, N., Yerli Tetik, N., Acar, E., Bekcioglu, O., and Baskin, Y. (2018). Difference between left-sided and right-sided colorectal cancer: a focused review of literature. Gastroenterology Res. *11*, 264–273. https://doi.org/10.14740/GR1062W.

9. Yui, S., Nakamura, T., Sato, T., Nemoto, Y., Mizutani, T., Zheng, X., Ichinose, S., Nagaishi, T., Okamoto, R., Tsuchiya, K., et al. (2012). Functional engraftment of colon epithelium expanded in vitro from a single adult Lgr5+ stem cell. Nat. Med. *184*, 618–623. https://doi.org/10.1038/nm.2695.

10. O'Rourke, K.P., Loizou, E., Livshits, G., Schatoff, E.M., Baslan, T., Manchado, E., Simon, J., Romesser, P.B., Leach, B., Han, T., et al. (2017). Transplantation of engineered organoids enables rapid generation of metastatic mouse models of colorectal cancer. Nat. Biotechnol. *35*, 577–582. https://doi.org/10.1038/NBT.3837.

11. Kasashima, H., Duran, A., Cid-Diaz, T., Muta, Y., Kinoshita, H., Batlle, E., Diaz-Meco, M.T., and Moscat, J. (2021). Mouse model of colorectal cancer: orthotopic co-implantation of tumor and stroma cells in cecum and rectum. STAR Protoc. *2*, 100297. https://doi.org/10.1016/J.XPRO.2021.100297.

12. Drost, J., van Jaarsveld, R.H., Ponsioen, B., Zimberlin, C., van Boxtel, R., Buijs, A., Sachs, N., Overmeer, R.M., Offerhaus, G.J., Begthel, H., et al. (2015). Sequential cancer mutations in cultured human intestinal stem cells. Nature *521*, 43–47. https://doi.org/10.1038/NATURE14415.

13. Rivera, M., Fichtner, I., Wulf-Goldenberg, A., Sers, C., Merk, J., Patone, G., Alp, K.M., Kanashova, T., Mertins, P., Hoffmann, J., et al. (2021). Patient-derived xenograft (PDX) models of colorectal carcinoma (CRC) as a platform for chemosensitivity and biomarker analysis in personalized medicine. Neoplasia *23*, 21–35. https://doi.org/10.1016/J.NEO.2020.11.005.

14. Tanaka, Y., Wu, A.Y., Ikekawa, N., Iseki, K., Kawai, M., and Kobayashi, Y. (1994). Inhibition of HT-29 human colon cancer growth under the renal capsule of severe combined immunodeficient mice by an analogue of 1, 25-Dihydroxyvitamin D3, DD-003. Cancer Res. *54*, 5148–5153.

15. Schoffelen, R., van der Graaf, W.T.A., Sharkey, R.M., Franssen, G.M., McBride, W.J., Chang, C.H., Bos, D.L., Goldenberg, D.M., Oyen, W.J.G., and Boerman, O.C. (2012). Quantitative immuno-SPECT monitoring of pretargeted radioimmunotherapy with a bispecific antibody in an intraperitoneal nude mouse model of human colon cancer. J. Nucl. Med. *53*, 1926–1932. https://doi.org/10.2967/JNUMED.112.106278.

16. Fumagalli, A., Suijkerbuijk, S.J.E., Begthel, H., Beerling, E., Oost, K.C., Snippert, H.J., van Rheenen, J., and Drost, J. (2018). A surgical orthotopic organoid transplantation approach in mice to visualize and study colorectal cancer progression. Nat. Protoc. *13*, 235–247. https://doi.org/10.1038/NPROT.2017.137.

17. Tanaka, T., Kohno, H., Suzuki, R., Yamada, Y., Sugie, S., and Mori, H. (2003). A novel inflammation-related mouse colon carcinogenesis model induced by azoxymethane and dextran sodium sulfate. Cancer Sci. *94*, 965–973. https://doi.org/10.1111/J.1349-7006.2003.TB01386.X.

18. Neufert, C., Becker, C., and Neurath, M.F. (2007). An inducible mouse model of colon carcinogenesis for the analysis of sporadic and inflammation-driven tumor progression. Nat. Protoc. *28*, 1998–2004. https://doi.org/10.1038/nprot.2007.279.

19. Xue, Y., Johnson, R., Desmet, M., Snyder, P.W., and Fleet, J.C. (2010). Generation of a transgenic mouse for colorectal cancer research with intestinal cre expression limited to the large intestine. Mol. Cancer Res. *8*, 1095–1104. https://doi.org/10.1158/1541-7786.MCR-10-0195.

20. Dow, L.E., O'Rourke, K.P., Simon, J., Tschaharganeh, D.F., van Es, J.H., Clevers, H., and Lowe, S.W. (2015). Apc restoration promotes cellular differentiation and reestablishes crypt homeostasis in colorectal cancer. Cell *161*, 1539–1552. https://doi.org/10.1016/J.CELL.2015.05.033.

21. Hung, K.E., Maricevich, M.A., Richard, L.G., Chen, W.Y., Richardson, M.P., Kunin, A., Bronson, R.T., Mahmood, U., and Kucherlapati, R. (2010). Development of a mouse model for sporadic and metastatic colon tumors and its use in assessing drug treatment. Proc. Natl. Acad. Sci. USA *107*, 1565–1570. https://doi.org/10.1073/PNAS.0908682107.

22. Roper, J., Tammela, T., Cetinbas, N.M., Akkad, A., Roghanian, A., Rickelt, S., Almeqdadi, M., Wu, K., Oberli, M.A., Sánchez-Rivera, F.J., et al. (2017). In vivo genome editing and organoid transplantation models of colorectal cancer and metastasis. Nat. Biotechnol. *35*, 569–576. https://doi.org/10.1038/NBT.3836.

23. Bettenworth, D., Mücke, M.M., Schwegmann, K., Faust, A., Poremba, C., Schäfers, M., Domagk, D., and Lenz, P. (2016). Endoscopy-guided orthotopic implantation of colorectal cancer cells results in metastatic colorectal cancer in mice. Clin. Exp. Metastasis *33*, 551–562. https://doi.org/10.1007/S10585-016-9797-7.

24. Roper, J., Tammela, T., Akkad, A., Almeqdadi, M., Santos, S.B., Jacks, T., and Yilmaz, Ö.H. (2018). Colonoscopy-based colorectal cancer modeling in mice with CRISPR-Cas9 genome editing and organoid transplantation. Nat. Protoc. *13*, 217–234. https://doi.org/10.1038/NPROT.2017.136.

25. Kishimoto, H., Momiyama, M., Aki, R., Kimura, H., Suetsugu, A., Bouvet, M., Fujiwara, T., and Hoffman, R.M. (2013). Development of a clinically-precise mouse model of rectal cancer. PLoS One *8*, e79453. https://doi.org/10.1371/JOURNAL.PONE.0079453.

26. Ganesh, K., Wu, C., O'Rourke, K.P., Szeglin, B.C., Zheng, Y., Sauvé, C.E.G., Adileh, M., Wasserman, I., Marco, M.R., Kim, A.S., et al. (2019). A rectal cancer organoid platform to study individual responses to

chemoradiation. Nat. Med. *25*, 1607–1614. https://doi.org/10.1038/s41591-019-0584-2.

27. Takahashi, T., Morotomi, M., and Nomoto, K. (2004). A novel mouse model of rectal cancer established by orthotopic implantation of colon cancer cells. Cancer Sci. *95*, 514–519. https://doi.org/10.1111/J.1349-7006.2004.TB03242.X.

28. Chassaing, B., Aitken, J.D., Malleshappa, M., and Vijay-Kumar, M. (2014). Dextran sulfate sodium (DSS)-induced colitis in mice. Curr. Protoc. Immunol. *104*, 15.25.1–15.25.14. https://doi.org/10.1002/0471142735.IM1525S104.

29. Hite, N., Klinger, A., Hellmers, L., Maresh, G.A., Miller, P.E., Zhang, X., Li, L., and Margolin, D.A. (2018). An optimal orthotopic mouse model for human colorectal cancer primary tumor growth and spontaneous metastasis. Dis. Colon Rectum *61*, 698–705. https://doi.org/10.1097/DCR.0000000000001096.

30. Ellsworth, S.G. (2018). Field size effects on the risk and severity of treatment-induced lymphopenia in patients undergoing radiation therapy for solid tumors. Adv. Radiat. Oncol. *3*, 512–519. https://doi.org/10.1016/J.ADRO.2018.08.014.

31. Romesser, P.B., Kim, A.S., Jeong, J., Mayle, A., Dow, L.E., and Lowe, S.W. (2019). Preclinical murine platform to evaluate therapeutic countermeasures against radiation-induced gastrointestinal syndrome. Proc. Natl. Acad. Sci. USA *116*, 20672–20678. https://doi.org/10.1073/PNAS.1906611116.

32. Nicolas, A.M., Pesic, M., Engel, E., Ziegler, P.K., Diefenhardt, M., Kennel, K.B., Buettner, F., Conche, C., Petrocelli, V., Elwakeel, E., et al. (2022). Inflammatory fibroblasts mediate resistance to neoadjuvant therapy in rectal cancer. Cancer Cell *40*, 168–184. https://doi.org/10.1016/J.CCELL.2022.01.004/ATTACHMENT/870044AC-C0E7-4432-BF15-535D49B8BCA6/MMC4.XLSX.

33. Rodríguez-Ruiz, M.E., Rodríguez, I., Mayorga, L., Labiano, T., Barbes, B., Etxeberria, I., Ponz-Sarvise, M., Azpilikueta, A., Bolaños, E., Sanmamed, M.F., et al. (2019). TGFb blockade enhances radiotherapy abscopal efficacy effects in combination with anti-PD1 and anti-CD137 immunostimulatory monoclonal antibodies. Mol. Cancer Ther. *18*, 621–631. https://doi.org/10.1158/1535-7163.MCT-18-0558/87711/AM/TGF-BLOCKADE-ENHANCES-RADIOTHERAPY-ABSCOPAL.

34. Smith, G., Carey, F.A., Beattie, J., Wilkie, M.J.V., Lightfoot, T.J., Coxhead, J., Garner, R.C., Steele, R.J.C., and Wolf, C.R. (2002). Mutations in APC, Kirsten-ras, and p53 - alternative genetic pathways to colorectal cancer. Proc. Natl. Acad. Sci. USA *99*, 9433–9438. https://doi.org/10.1073/PNAS.122612899/SUPPL_FILE/6128FIG5B.JPG.

35. Vidal-Lletjós, S., Andriamihaja, M., Blais, A., Grauso, M., Lepage, P., Davila, A.M., Gaudichon, C., Leclerc, M., Blachier, F., and Lan, A. (2019). Mucosal healing progression after acute colitis in mice. World J. Gastroenterol. *25*, 3572–3589. https://doi.org/10.3748/WJG.V25.I27.3572.

36. Uchihashi, M., Wilding, L.A., and Nowland, M.H. (2015). Surgical correction of rectal prolapse in laboratory mice (Mus musculus). J. Am. Assoc. Lab. Anim. Sci. *54*, 433–438.

37. Ryan, R., Gibbons, D., Hyland, J.M.P., Treanor, D., White, A., Mulcahy, H.E., O'Donoghue, D.P., Moriarty, M., Fennelly, D., and Sheahan, K. (2005). Pathological response following long-course neoadjuvant chemo-radiotherapy for locally advanced rectal cancer. Histopathology *47*, 141–146. https://doi.org/10.1111/J.1365-2559.2005.02176.X.

38. Trakarnsanga, A., Gönen, M., Shia, J., Nash, G.M., Temple, L.K., Guillem, J.G., Paty, P.B., Goodman, K.A., Wu, A., Gollub, M., et al. (2014). Comparison of tumor regression grade systems for locally advanced rectal cancer after multimodality treatment. J. Natl. Cancer Inst. *106*, dju248. https://doi.org/10.1093/JNCI/DJU248.

39. Yasui, K., Kondou, R., Iizuka, A., Miyata, H., Tanaka, E., Ashizawa, T., Nagashima, T., Ohshima, K., Urakami, K., Kusuhara, M., et al. (2020). Effect of preoperative chemoradiotherapy on the immunological status of rectal cancer patients. J. Radiat. Res. *61*, 766–775. https://doi.org/10.1093/JRR/RRAA041.

40. Vuik, F.E., Nieuwenburg, S.A., Bardou, M., Lansdorp-Vogelaar, I., Dinis-Ribeiro, M., Bento, M.J., Zadnik, V., Pellisé, M., Esteban, L., Kaminski, M.F., et al. (2019). Increasing incidence of colorectal cancer in young adults in Europe over the last 25 years. Gut *68*, 1820–1826. https://doi.org/10.1136/GUTJNL-2018-317592.

41. Araghi, M., Soerjomataram, I., Bardot, A., Ferlay, J., Cabasag, C.J., Morrison, D.S., De, P., Tervonen, H., Walsh, P.M., Bucher, O., et al. (2019). Changes in colorectal cancer incidence in seven high-income countries: a population-based study. Lancet. Gastroenterol. Hepatol. *4*, 511–518. https://doi.org/10.1016/S2468-1253(19)30147-5.

42. Siegel, R.L., Fedewa, S.A., Anderson, W.F., Miller, K.D., Ma, J., Rosenberg, P.S., and Jemal, A. (2017). Colorectal cancer incidence patterns in the United States, 1974-2013. J. Natl. Cancer Inst. *109*. https://doi.org/10.1093/JNCI/DJW322.

43. Willauer, A.N., Liu, Y., Pereira, A.A.L., Lam, M., Morris, J.S., Raghav, K.P.S., Morris, V.K., Menter, D., Broaddus, R., Meric-Bernstam, F., et al. (2019). Clinical and molecular characterization of early-onset colorectal cancer. Cancer *125*, 2002–2010. https://doi.org/10.1002/CNCR.31994.

44. Hofseth, L.J., Hebert, J.R., Chanda, A., Chen, H., Love, B.L., Pena, M.M., Murphy, E.A., Sajish, M., Sheth, A., Buckhaults, P.J., and Berger, F.G. (2020). Early-onset colorectal cancer: initial clues and current views. Nat. Rev. Gastroenterol. Hepatol. *17*, 352–364. https://doi.org/10.1038/S41575-019-0253-4.

45. Keum, N., and Giovannucci, E. (2019). Global burden of colorectal cancer: emerging trends, risk factors and prevention strategies. Nat. Rev. Gastroenterol. Hepatol. *16*, 713–732. https://doi.org/10.1038/s41575-019-0189-8.

46. Xi, Y., and Xu, P. (2021). Global colorectal cancer burden in 2020 and projections to 2040. Transl. Oncol. *14*, 101174. https://doi.org/10.1016/J.TRANON.2021.101174.

47. Yaeger, R., Shah, M.A., Miller, V.A., Kelsen, J.R., Wang, K., Heins, Z.J., Ross, J.S., He, Y., Sanford, E., Yantiss, R.K., et al. (2016). Genomic alterations observed in colitis-associated cancers are distinct from those found in sporadic colorectal cancers and vary by type of inflammatory bowel disease. Gastroenterology *151*, 278–287.e6. https://doi.org/10.1053/J.GASTRO.2016.04.001.

48. Leary, S., and Johnson, C.L. (2020). AVMA GUIDELINES for the EUTHANASIA of ANIMALS: 2020 EDITION AVMA Guidelines for the Euthanasia of Animals: 2020 Edition (American Veterinary Medical Association). https://www.avma.org/sites/default/files/2020-02/Guidelines-on-Euthanasia-2020.pdf.

STAR★METHODS

KEY RESOURCES TABLE

REAGENT or RESOURCE	SOURCE	IDENTIFIER
Antibodies		
Rabbit anti-mouse CD206 polyclonal antibody	Abcam	Cat# 64693, RRID:AB_1523910
Armenian hamster anti-mouse CD11c monoclonal antibody, clone N418	eBioscience	Cat# 14-0114-82
Rabbit anti-mouse CD4 monoclonal antibody, clone EPR19514	Abcam	Cat# ab183685, RRID:AB_2686917
Rat anti-mouse CD8 monoclonal antibody, clone 4SM15	eBioscience	Cat# 14-0808-80
Rat anti-mouse FOXP3 monoclonal antibody, clone FJK-16s	Invitrogen	Cat# 14-5773-82
Rat anti-mouse F4/80-Alexa Fluor 594 monoclonal antibody, clone BM8	Biolegend	Cat# 123140; RRID:AB_2563241
Goat anti-human E-cadherin polyclonal antibody	R&D	Cat# AF748; RRID:AB_355568
Rabbit anti-human phospho-p44/42 MAPK (Erk1/2) monoclonal antibody, clone D12.14.4E	Cell Signaling	Cat# 4370; RRID:AB_2315112
Rabbit anti-human β-Catenin monoclonal antibody, clone E247	Abcam	Cat# Ab32572; RRID:AB_725966
Donkey anti-rabbit secondary antibody, Alexa Fluor 488	Invitrogen	Cat# A-21206
Goat anti-Armenian hamster secondary antibody, Alexa Fluor 488	Invitrogen	Cat# A-21110
Donkey anti-Rat secondary, Alexa Fluor 594	Invitrogen	Cat# A-21209
Donkey anti-rabbit secondary antibody, Alexa Fluor 647	Invitrogen	Cat# A-31573
Donkey anti-goat secondary antibody, Alexa Fluor 647	Invitrogen	Cat# A-21447
Rat IgG2a-Alexa Fluor 594 isotype control	Biolegend	400555
Rabbit IgG isotype control	Abcam	Cat# ab172730; RRID:AB_2687931
Rat IgG2a isotype control	R&D	Cat# MAB006; RRID:AB_357349
Armenian Hamster IgG isotype control	eBioscience	Cat# 14-4888-81
Bacterial and virus strains		
Ad-CMV-iCre	Vector BioLabs	1045
Chemicals, peptides, and recombinant proteins		
Advanced DMEM/F12	Thermo Fisher Scientific	12634-010
Penicillin–streptomycin	Thermo Fisher Scientific	15140-122
HEPES	Quality Biological	118-089-721
GlutaMAX supplement	Thermo Fisher Scientific	35050-061
N-acetyl-L-cysteine (NAC)	Sigma-Aldrich	A9165
Nicotinamide	Sigma-Aldrich	N0636
Bovine serum albumin (BSA)	Sigma-Aldrich	A2058
Recombinant murine EGF (mEGF)	Thermo Fisher Scientific	PMG8043
Dulbecco's Modified Eagle's Medium (DMEM)	ATCC	30-2002
Fetal Bovine Serum (FBS)	Sigma	F2442
B27 Supplement	Thermo Fisher Scientific	17504-044
Y27632 dihydrochloride	Sigma-Aldrich	Y0503
Matrigel, Growth factor reduced	Corning	356231
Cell Recovery Solution	Corning	354253
TrypLE Express Enzyme	Thermo Fisher Scientific	12605-010
PBS	Corning	21-031-CV
0.4% Trypan Blue solution	Sigma	T8154

(Continued on next page)

Continued

REAGENT or RESOURCE	SOURCE	IDENTIFIER
Matrigel, Basement	Corning	356237
Vetbond Tissue Adhesive	3M	1469SB
Hoechst 33342	Sigma	B2261
4′,6′-diamidino-2-phenylindole (DAPI)	Sigma-Aldrich	D9542
Zeocin	Gibco	R25001
Nutlin-3	Selleckchem	S1061
Experimental models: Cell lines		
Noggin	Kindly provided by the S. Lowe laboratory[10]	N/A
Wnt3a	Kindly provided by the S. Lowe laboratory[10]	N/A
293T-Rspondin	Kindly provided by the S. Lowe laboratory[10]	N/A
Experimental models: Organisms/strains		
Mouse: C57Bl/6J	The Jackson Laboratory	000664
Mouse: C57BL/6J, $Apc^{flox/flox}$ transgenic line	Maintained by the S. Lowe laboratory	N/A
Mouse: C57BL/6J, $LSL\text{-}Kras^{G12D/+}$ transgenic line	Maintained by the S. Lowe laboratory	N/A
Mouse: C57BL/6J, $Tp53^{flox/flox}$ transgenic line	Maintained by the S. Lowe laboratory	N/A
Other		
Cell culture dish, 150 mm	Falcon	353025
Suspension cell culture plate, 6-well	Greiner Bio-One	657185
Conical tube, 15 mL	VWR	525-1069
Conical tube, 50 mL	VWR	525-1074
0.2-mL tube	Fisherbrand	14-230-225
Microcentrifuge tube, 1.5 mL	Crystalgen	L2052
5-mL tube	Axygen	MCT-500-C
500-mL bottle-top vacuum filter, 0.22 μm	Corning	431118
60-mL syringe	BD	309653
0.45-μm syringe filter	Thermo Scientific	723-2545
10-mL syringe	BD	309604
Oral gavage needle	Roboz	FN 7905
Small caliber nylon brush (2.5 mm)	Karl Storz	27650C
1.9-mm rigid 30° small animal endoscope	Karl Storz	64301BA
X-Rad 320 machine	Precision X-ray	N/A

RESOURCE AVAILABILITY

Lead contact
Further information and requests for resources and reagents should be directed to and will be fulfilled by the lead contact, J. Joshua Smith MD PhD (smithj5@mskcc.org).

Materials availability
- This study did not generate new, unique reagents.
- There are restrictions to the availability of ketamine/xylazine due to federal, state, and institutional restrictions as this is a Schedule III substance under the Controlled Substances Act.
- Matrigel basement membrane is a limited resource due to high demand and backorder capacity. Protein concentration may vary slightly between batches. This can be normalized and controlled for using the manufacturer's batch-specific production information.

Data and code availability
- Endoscopic visualization of colorectal tumors and survival data reported in this paper will be shared by the lead contact upon request.
- This paper does not report original code.

● Any additional information required to reanalyze the data reported in this paper is available from the lead contact upon request.

EXPERIMENTAL MODEL AND SUBJECT DETAILS

Mice

We used 6- to 8-week-old female C57Bl/6J mice (Jackson Laboratory, stock no. 000664). All animal experiments were conducted under protocols 11-06-012 and 06-07-012 approved by the Memorial Sloan Kettering Cancer Center's Institutional Animal Care and Use Committee in conjunction with the Research Animal Resource Center and American Association (RARC) for Laboratory Animal Science (IACUC).

METHOD DETAILS

Step-by-step protocols and details on reagent preparation are provided in Supplemental methods S1. Reagents were used freshly, and nothing more than 6 months old or expired was used.

Culturing and preparation of tumoroids for endoluminal transplantation

AKP tumoroids were derived, cultured, and prepared for endoluminal transplantation as described.[10,15] Cells were released from Matrigel and resuspended in ice-cold PBS with 5% Matrigel to a concentration of 2×10^5 cells/100 μL per mouse.

Mechanical disruption of the mouse rectal mucosa and tumoroid transplantation

Critical steps are shown in Video S1. Anesthetized mice (2% isoflurane and oxygen) underwent rectal flushing to expel stool using PBS. A smooth-trimmed P200 pipette tip (lubricated with Vaseline) was inserted into the anus as guide, then a small-caliber brush was inserted through the pipette tip and moved gently in to and out of the rectum 3–5 times to gently disrupt the rectal mucosa. The tumoroid suspension was then slowly injected transanally using a P200 pipette. The anus was sealed using 3 μL of Vetbond Tissue Adhesive to prevent luminal contents from spilling. This bond was removed between 6 and 8 h later.

Tumor surveillance and measuring tumor growth

Tumor engraftment was monitored by 1.9-mm rigid 30° small animal endoscope weekly. A video of each endoscopy was taken, and a static picture of the tumor was analyzed to calculate endoluminal involvement. Tumor growth was quantified by the percent of the field of view occupied by the tumor area as described.[26]

Localized pelvic radiation

Mice were anesthetized by intraperitoneal injection of Ketamine/Xylazine (100 mg/mL; 10 μL/g body weight). Localized pelvic irradiation was delivered using an X-Rad 320 machine (Precision X-ray, Madison, CT) (250kVp/12mA) with customized Cerrobend blocks. The fabrication technique for this apparatus can be shared upon request.

Histopathology

Dissected tumor samples were fixed with 4% paraformaldehyde, embedded in paraffin, and sectioned according to standard protocols. For histopathologic evaluation, 5-μm sections were stained with H&E.

Immunofluorescence

Tissue sections were deparaffinized, then boiled in pH 6.1 citrate buffer for 20 min for antigen retrieval. Sections were blocked in 10% normal donkey serum and 1% BSA at room temperature for 1 h, immunostained overnight at 4°C with primary antibodies, then for 2 h at room temperature with fluorophore-conjugated secondary antibodies. Cell nuclei were labeled with DAPI or Hoechst, as noted.

Imaging

Slides were scanned by a Panoramic Flash slide scanner using a 20 ×0.8 NA objective. Images were examined and representative areas exported using CaseViewer 2.2. No gamma changes were made to any immunofluorescence images. All brightfield images are unaltered. Immune cells in total tumor regions were quantified using custom macros written in ImageJ (NIH, Bethesda, MD, USA). The number of immune cells in 1mm[41] of tumor regions were calculated from each sample and averaged per group, and a Student's *t* test was performed for statistical analysis.

Monitoring mouse health

Upon arrival, mice are weighed and observed to confirm robust health prior to implantation. After implantation, mice are observed for 5 min to ensure return to normal levels of body condition, activity, and alertness. Six to 8 h after implantation any remaining Vetbond is

removed. Once a day for three days post-procedure, mice are observed again. Past this period, mice are monitored once a week through general observation and tumors surveilled by endoscopic imaging.

Adherence to established endpoints

Mice exhibiting excessive weight loss (>20% decrease from baseline), decreased activity, worsening body condition, reduced alertness, and/or blunted response to stimulation and handling were eligible for euthanasia. Mortality from perforation due to excessive epithelial disruption is most frequently observed <24h post-implantation. For mice developing rectal tumors, if circumferential lumen involvement exceeded 50% or if tumor growth interfered with ambulation, eating, drinking, defecation, or urination, mice were euthanized. While we did not observe rectal prolapse in our mice, likely due to close endoscopic monitoring, it is known that rectal prolapse can occur with large obstructing tumors and mice should be monitored for this closely. Standard, pre-approved institutional methods of CO_2 overdose and asphyxiation were used to euthanize mice as outlined by the *RARC's Recommended Methods of Euthanasia for Laboratory Animals*.[48]

QUANTIFICATION AND STATISTICAL ANALYSIS

The number of biological replicates per experiment and the number of experiments performed for each dataset and the statistical analysis performed are outlined in the corresponding figure legends. Results are depicted as mean ± standard deviation (SD) unless otherwise stated using Microsoft Excel for Mac (v16.56) or GraphPad Prism (v.9.3.1). P-values were calculated using GraphPad Prism (v.9.3.1) and Microsoft Excel for Mac (v16.55). No statistical method was used to predetermine sample size. Sample sizes were estimated according to transplantation success and previous pilot experiments to estimate variability.